Wireless Netw
DOI 10.1007/s11276-007-0040-y

Free-space-optical mobile ad hoc networks: Auto-configurable building blocks

**Murat Yuksel · Jayasri Akella ·
Shivkumar Kalyanaraman · Partha Dutta**

Abstract Existence of line of sight (LOS) and alignment between the communicating antennas is one of the key requirements for free-space-optical (FSO) communication. To ensure uninterrupted data flow, auto-aligning transmitter and receiver modules are necessary. We propose a new FSO node design that uses spherical surfaces covered with transmitter and receiver modules for maintaining optical links even when nodes are in relative motion. The spherical FSO node provides angular diversity in 3-dimensions, and hence provides an LOS at any orientation as long as there are no obstacles in between the communicating nodes. For proof-of-concept, we designed and tested an auto-configurable circuit, integrated with light sources and detectors placed on spherical surfaces. We demonstrated communication between a stationary and a mobile node using these initial prototypes of such FSO structures. We also performed the necessary theoretical analysis to demonstrate scalability of our FSO node designs to longer distances as well as feasibility of denser packaging of transceivers on such nodes.

M. Yuksel (✉)
University of Nevada – Reno, CSE Department,
MS 171, 1664 N. Virginia Street, Reno, NV 89557, USA
e-mail: yuksem@cse.unr.edu

J. Akella · S. Kalyanaraman · P. Dutta
Rensselaer Polytechnic Institute, ECSE Department,
JEC 6049, 110 8th Street, Troy, NY 12180, USA

J. Akella
e-mail: akellj@rpi.edu

S. Kalyanaraman
e-mail: shivkuma@ecse.rpi.edu

P. Dutta
e-mail: duttap@rpi.edu

Keywords Free space optical communication · Auto-configurable · Angular diversity

1 Introduction

Optical wireless, also known as free space optics (FSO), is an effective high bandwidth communication technology serving commercial point-to-point links in terrestrial last mile applications and in infrared indoor LANs [1, 3, 11, 13, 27, 28]. FSO has several attractive characteristics like license-free band of operation, dense spatial reuse, low power usage per transmitted bit, and relatively high bandwidth. However, one of the major limitations of FSO is line of sight (LOS) maintenance for continuous data flow. Current FSO equipment is targeted at point-to-point links using high-powered lasers and relatively expensive components used in fiber-optical transmission. Mobile communication using FSO is considered for indoor environments, within a single room, using diffuse optics technology [7, 8, 11, 13, 18, 24, 30]. Due to limited power of a single source that is being diffused to spread in all directions, these techniques are suitable for small distances (typically 10 s of meters), but not suitable for longer distances. For outdoors, fixed FSO communication techniques to remedy small vibrations [4, 5], swaying of the buildings have been implemented using mechanical auto-tracking [2, 6, 17] or beam steering [29], and interference [16] and noise [26]. Similarly, for optical interconnects, auto-alignment or wavelength diversity techniques are reported to improve the misalignment tolerances in 2-dimensional arrays [9, 10, 12, 14, 19]. These techniques work only over small ranges (e.g. 1 μm–1 cm) and some of these are cumbersome involving heavy mechanical tracking instruments. Moreover, they are designed to improve the tolerance to movement and vibration but not to handle mobility. Thus, *mobile* FSO communication

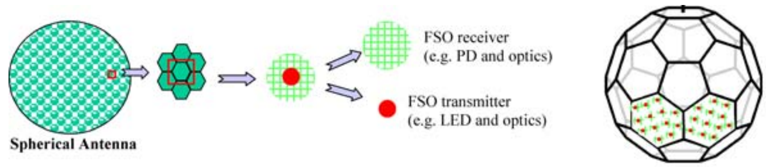

(a) Tessellated sphere

(b) Honeycombed arrays of transceivers

Fig. 1 *3-d spherical FSO systems tessellated with optical transceivers*: Spherical surface provides angular diversity and nice coverage with almost omni-directional LOS capabilities. Dense packaging of transceivers using cheap optoelectronic components as well as both single and arrays of such transceivers on honeycombed cells are possible

has not been realized, particularly for ad hoc networking and communication environments.

In order to enable FSO communication in mobile environments, we introduce the concept of a spherical FSO node that provides angular diversity and hence LOS in all directions. Figure 1 shows the general concept of spherical surfaces being tessellated with FSO transceivers, i.e. a pair of optical transmitter (e.g. Light Emitting Diode (LED)) and optical receiver (e.g. Photo-Detector (PD)). For the design of an FSO transceiver, it is desirable to have the size of the transmitter as small as possible and the receiver as large as possible to minimize the geometric loss due to beam divergence of the optical beam. Taking this point into consideration, we fixed the size of the central transmitter area at a typical size of an LED (i.e. 2 mm), and increase the size of the receiver area, as we increase the total transceiver area (illustrated in the Fig. 14 and Fig. 1(a)). This larger area of the transceiver can be achieved by the use of optics (collimating lens etc.) in front of the PD or by use of multiple PDs or both depending on the application.

Such spherical FSO nodes use multiple optical transceivers tessellated on the surface of a sphere. The tessellation not only improves the range characteristics because every direction now has a light source (e.g. an LED) whose operating range is typically up to a few hundred meters (though special designs can reach up to a few kilometers by aggregation of multiple LEDS or VCSELs [31]), but also enables multi-channel simultaneous communication through multiple transceivers. As shown in Fig. 1(b), tradeoffs between spatial reuse and angular diversity can be obtained by constructing the FSO node as honeycombed arrays of transceivers.

In this paper, to illustrate feasibility of above-mentioned spherical FSO nodes, we design an auto-alignment circuit that electronically tracks the light beams to maintain continuous LOS between two communicating optical nodes even when they are mobile, and demonstrate the mobility in a two-node proto-type experiment.

We also show through theoretical modeling that these FSO node designs can allow very dense packaging and scale to very long communication ranges as well as coverage (e.g. a 2 cm radius FSO node with transceivers of radius 1 cm and source power 32 m Watts can cover a total of 484.5 m^2 in adverse weather and 979.5 m^2 in clear weather). Our modeling of the proposed spherical FSO node revealed that the source power at transmitters and the visibility have little or no effect on the optimality of the number of transceivers on such structures. Rather, the geometric shape of the FSO node and the divergence angle play the major role, which means that adaptive tuning of the source power based on the actual visibility is possible without having to change the physical number of transceivers on these FSO nodes. This is an important result since it means that optimum number of transceivers is *fixed* for a particular FSO node design. *To the best of our knowledge, this is the first time spatial reuse and angular diversity coupled with electronic tracking (i.e. auto-alignment) for "mobile" communications using free space optical technology is being reported.*

2 Background

Though some preliminary multi-hop proposals exist, current FSO equipment is targeted at point-to-point links using high-powered lasers and relatively expensive components used in fiber-optical transmission. The focus of these commercial systems (e.g. Terabeam [25] and LightPointe [15]) is to form a single primary beam (and some backup beams) with limited spatial re-use/redundancy and to push the limits of operating range, and to improve link availability during poor conditions [19]. We instead focus on solving the LOS alignment problem with dense packaging of transceiver elements, enabling mobility through circular or spherical auto-configuring FSO systems, and target shorter per hop distances.

In commercial FSO systems, lasers in the 850 nm and 1550 nm band are preferred due to superior propagation characteristics in this band and higher power budget due to low geometric dispersion. Such equipment would be very costly and demands high-power in the context of multi-element scenario. Moreover, such laser-based equipment would not have the form factor, weight and power characteristics to be mounted on ad-hoc infrastructures. We instead investigate FSO systems using models of LEDs in our design as they are more amenable to dense and spatial packaging, and have longer life than lasers and fewer eye-safety regulations.

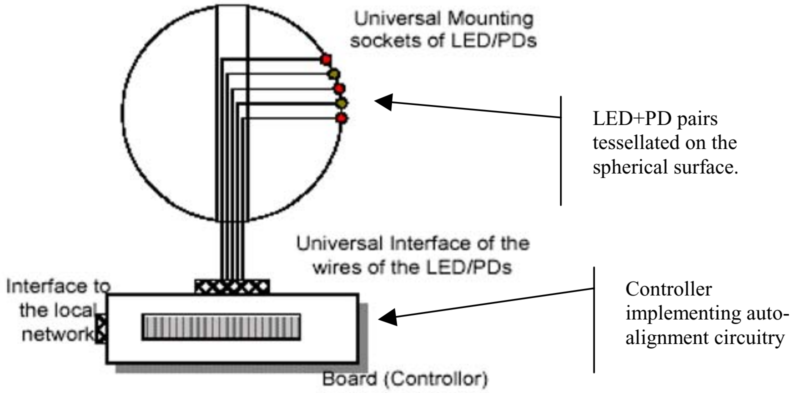

Fig. 2 *A schematic of the 3-d spherical FSO node design*: Spherical surface is tessellated with LED + PD pairs, and an auto-alignment circuit is implemented on the controller of the system

High-brightness LED technology is being rapidly developed in the context of solid-state lighting [23, 28]. Similarly, VCSELs are also very low-cost and provide high reliability. VCSELs and LEDs can be internally modulated at rates up to 2 Gbps [11], and spatial packaging of hundreds of such devices can yield very high aggregate transmission capacities. Recently, wireless communications using high speed LEDs have been reported [21] and several optimizations to their setup are possible for higher bandwidth operation.

3 Auto-configurable FSO node design

Auto-configurability of our FSO systems is based on two fundamental design components: (i) spherical surface tessellated with transceivers, and (ii) auto-alignment circuitry. As shown in Fig. 2, the spherical surface provides angular diversity in receiving/transmitting optical signals in a virtually omni-directional manner, and the auto-alignment circuit selects which transceiver to use for data communication. We now detail these two components in the following subsections.

3.1 The concept of tessellated spherical surfaces

The geometric shape of a sphere suggests *spatial reuse* and *angular diversity*. We tessellated the surface of the sphere using optical transceivers each of which contains an LED (Light Emitting Diode) as the transmitter and a photo detector (PD) as the receiver. Since LEDs have relatively high divergence angle and PDs have a comparable angular field of view, the LED-PD pair forms a transceiver cone. This cone covers a significant volume of 3-dimensional space. As shown in Fig. 1(b), a sphere tessellated to an appropriate density can cover entire 360° steradian of the surrounding space. As seen from the Fig. 3, when the spheres move relative to each other, an existing LOS between them is lost and a new one is established.

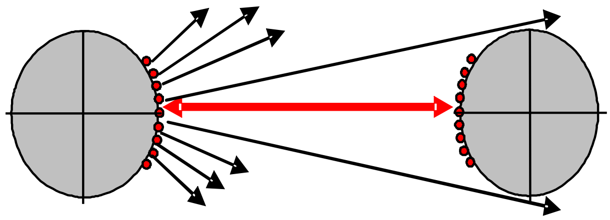

Fig. 3 *3-d spherical FSO node showing a line of sight (LOS)*: Two spheres in LOS can potentially communicate even if they move in relation to each other. Even though LOS is lost at the previous transceivers, LOS can be quickly recovered through new transceivers located at other parts of the spheres

3.2 Auto-alignment circuit

The basic functionality of the auto-alignment circuit is to monitor the incoming light beams at each transceiver and maintain continuous communication between two mobile FSO nodes by dynamically latching appropriate transceivers within their LOS. Figure 4 shows the schematic of the circuit for two spherical FSO nodes with four transceivers.

In the event of misalignment, the circuit first (i) searches for an existing LOS between the two spheres, and then (ii) continues data communication through the new LOS, once a new LOS is established. These two functionalities are implemented in a common hardware for all the transceivers on a single spherical FSO node. The part of the circuit that monitors an existing LOS is shown as the "LOS Unit", which gives out a logical high output when an LOS is present between the two communicating nodes and a logical low input when the LOS is lost. The logical low output triggers the "LOS search". During this phase, data transmission is temporarily aborted and search pulses are sent out in all the directions looking for LOS. The second sphere, which now moved to a different location, also drops LOS and hence it too starts to initiate LOS searching. The spheres eventually receive the search pulses upon existence of a new LOS, which causes first a high output from the LOS Unit and then restoration of the data transmission.

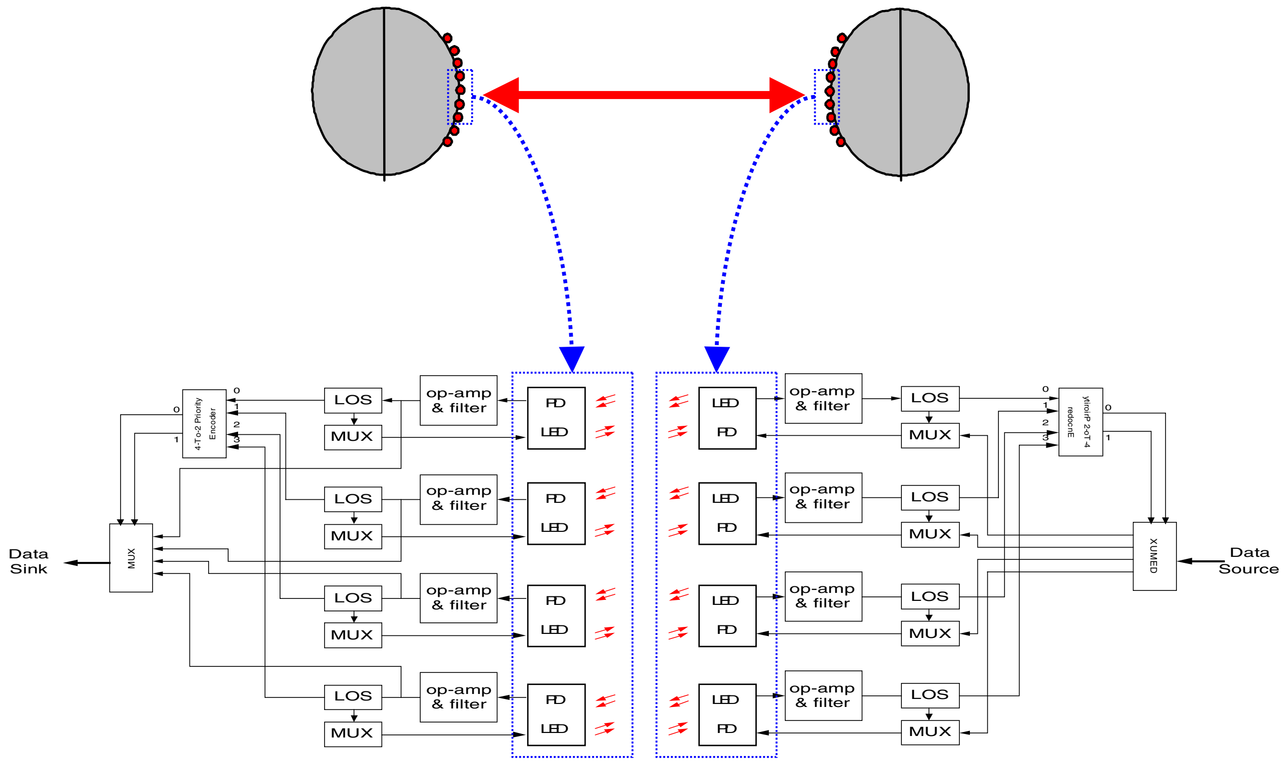

Fig. 4 *Schematic of the auto-alignment circuit with 4 physical channels*: Four transceivers exist on each FSO node, and each of the four transceivers is connected to appropriate circuitry to automatically select the proper transceiver for communication in case of LOS

For cases when multiple channels are aligned, we used a priority decoder to select a channel via the LOS signals from each transceiver. When no channel is aligned, the system searches for alignment by sending pulses to each channel. As soon as one or more channels get aligned, it starts to send the data signal out through the aligned channel. Thus, the logical data channel (or stream) is assigned to the physical channels dynamically depending on whether or not they are aligned. Several improvements (e.g. selection of the best transceiver when multiple ones are aligned) to this system are possible; however we are presenting a proof-of-concept experimentation in this paper.

4 Mobility analysis

We performed an experiment to demonstrate the concept of spatial reuse and LOS auto-alignment in the case when multi-channels are aligned. We built one cylindrical and one planar FSO node with 4 duplex optical channels on each. Each optical transceiver included an LED with a divergence angle of 24° and a PD with field of view of 20°. We spaced four transceivers on the cylindrical surface (which projects as a circular line in 2-dimensions) with an equal separation angle φ of 32° along a circumference normal to the cylinder axis. The planar surface also included four transceivers equally spaced along a line.

Using the cylindrical and planar surfaces, we then placed the planar surface as part of a train's cargo, and moved the train along a circular path of radius 30 cm around the cylindrical surface to create relative mobility. As the train moves the transceivers get aligned and misaligned. Figure 5(a) shows a misalignment instance in which the search pulses are sent out by all transceivers and LEDs are glowing. Figure 5(b) shows an instance of alignment in which two transceivers are in LOS with each other and data transmission is going through them. This pattern repeats as the train travels along the circular path. Figure 6 demonstrates the continuous alignment and misalignment phases as the train moves relative to the cylinder. For this setup, we used a light intensity threshold of 33.3 lux at PDs to determine LOS. Notice that, LOS periods can be increased by appropriately tuning the light intensity threshold at PDs, the divergence angles of LEDs, the field of view angles of PDs, and by increasing tessellation density. The speed of the circuit should be more than the speed of the relative movement between the spheres so as to maintain a smooth data flow. Otherwise, the data will be either buffered or dropped. Design of such buffering and queuing techniques is an important research issue, which we will study in another paper.

To further analyze mobility in this experiment, we consider a train moving with an angular speed of ω radians/s. Given the light intensity profile in Fig. 6, we can draw a generic LOS plot as in Fig. 7 for an LOS Detection Unit

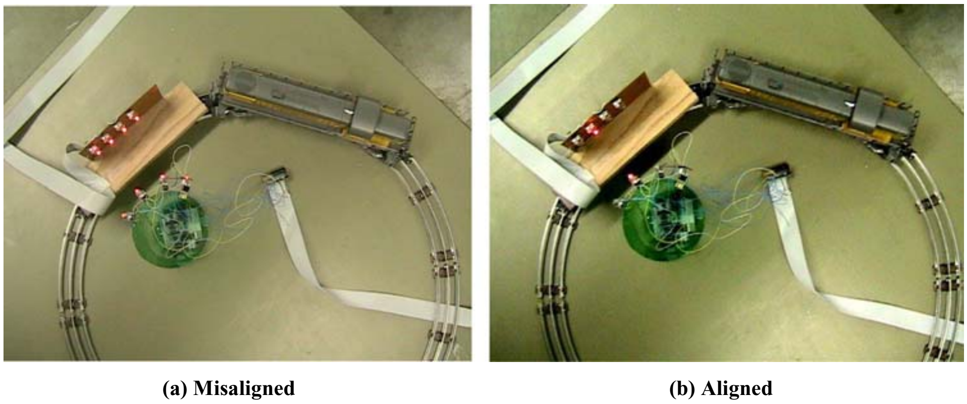

Fig. 5 *Illustration of the mobility experiment using a train*: All transceivers are sending search pulses when LOS is lost as in (a). But, only the selected transceiver sends/receives when an LOS is detected

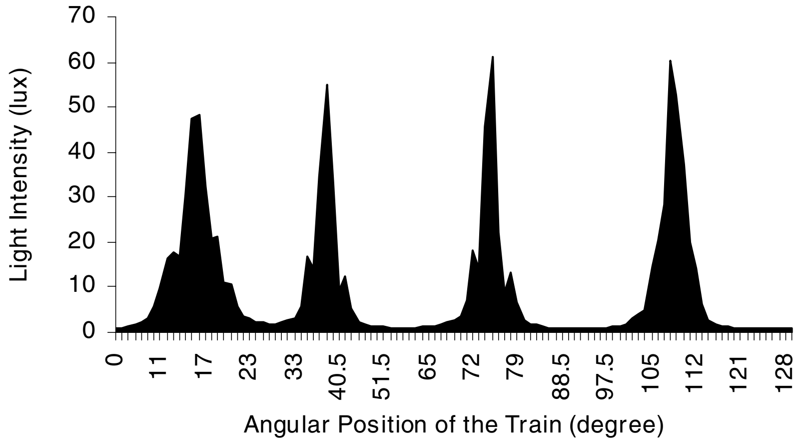

Fig. 6 Intensity received at the cylindrical FSO node as the train moves along the circle

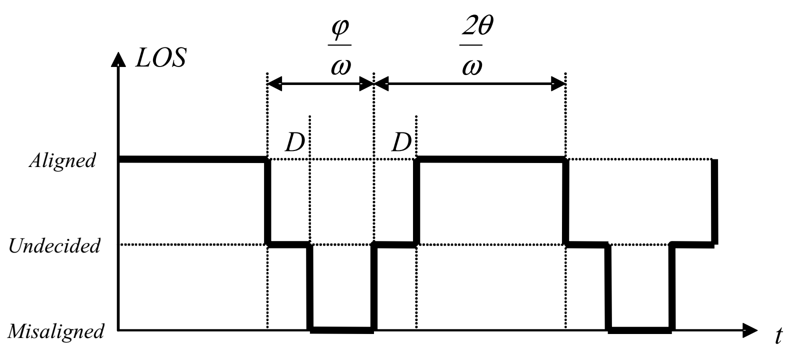

Fig. 7 LOS condition with respect to a train moving with an angular speed ω

with a delay D seconds. Here, the length of alignment period will depend on LED's divergence angle[1] θ and the train's speed ω; and the length of misalignment period will also depend on ω as well as density of tessellation which could be quantified as the angle φ during which alignment is lost. Notice that both θ and φ depends on LED's optical characteristics as well as the distance between the train and the stationary cylindrical FSO node.

Interestingly, in terms of the overall percentage of time the two FSO nodes are aligned, t_A, the train's speed will only affect the performance depending on the circuit delay. This relationship could be characterized as $t_A = 2\theta - D\omega/2\theta + \varphi$. To observe effects of the circuit delay and mobility, we have plotted t_A with respect to ω and D in Fig. 8. We have chosen $\varphi = 0.5°$ to see the behavior for a high density tessellation, and the divergence angle $\theta = 2°$ as it can be approximated

[1] Our divergence angle definition refers to the half angle from the axis of light propagation.

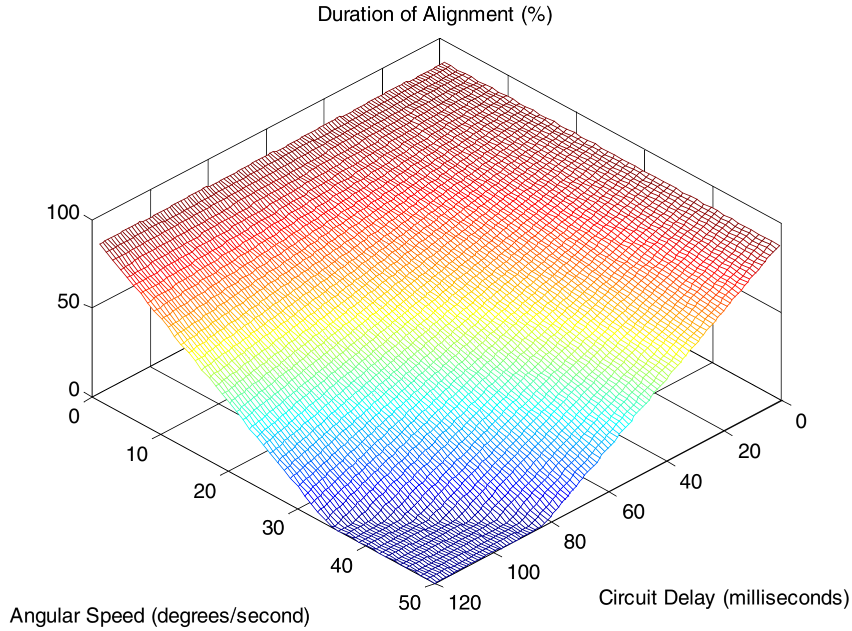

Fig. 8 System performance with respect to train's angular speed

from Fig. 6 for the LEDs we used. Notice the increased effect of mobility in performance when circuit delay is higher. It is worth noting that very high mobility is tolerable for very realistic circuit delay ranges, e.g. 50 degrees/s for less than 10 milliseconds circuit delay. Given that our experimental circuit had a delay about 200 ns, this result shows practicality of high-density tessellation of optical transceivers.

5 Optimum communication coverage

A crucial characteristic of RF communication is that it allows connectivity through large communication coverage areas at all directions since RF signals are omni-directional. The *coverage area* here refers to the area around the node, in which a communication link can be established with another node standing within the area of consideration. Having large coverage areas compensates higher mobility and allows more flexibility to the mobile nodes. In this section, we will investigate maximum communication coverage areas that can be attained by our FSO structures. Similar to RF, we will refer to coverage area as the area in which LOS and hence a communication link can be established with another spherical FSO node.

In spherical FSO nodes tessellated with multiple optical transceivers, there are tradeoffs involving (i) interference (or crosstalk) between the neighboring transceivers, (ii) aggregate coverage area achieved by the FSO node, (iii) packaging density of the optical transceivers, and (iv) communication range. Therefore, higher packaging density provides higher aggregate coverage but also increases the interference of the neighboring transceivers. An important design question is to ask how dense the packaging should be so that highest (or optimal) possible aggregate coverage is achieved without causing interference. The interference of the light beams received from multiple (most likely neighbor) transceivers can be particularly problematic during the LOS search and establishment phases as there is a need for distinguishing the light beams received from each of the contributing neighbor transceivers. In other words, what is the optimal number of transceivers to place on an FSO node to attain highest communication coverage? Another design tradeoff dimension is the communication range that can be achieved with such densely-packaged FSO nodes. If higher power is fed to the optical transmitters (e.g. LEDs) on the node, communication range increases; however, interference also increases at longer distances due to beam divergence. So, to investigate if the proposed FSO nodes can scale to long communication ranges, an analysis of how long communication ranges can be achieved is necessary.

In this section, to investigate the above-mentioned tradeoffs, we present our analysis of the scalability of the angular diversity and spatial reuse provided by a circular shaped FSO node. In particular, we answer the question of how much coverage can be achieved by a *2-d circular FSO node* with the highest possible number of transceivers. To find the optimal number of transceivers maximizing the total coverage of a 2-d circular FSO node, we first develop the model for total coverage area of such a node. Then, we devise an iterative algorithm to find the optimal number of transceivers that maximize the total coverage.

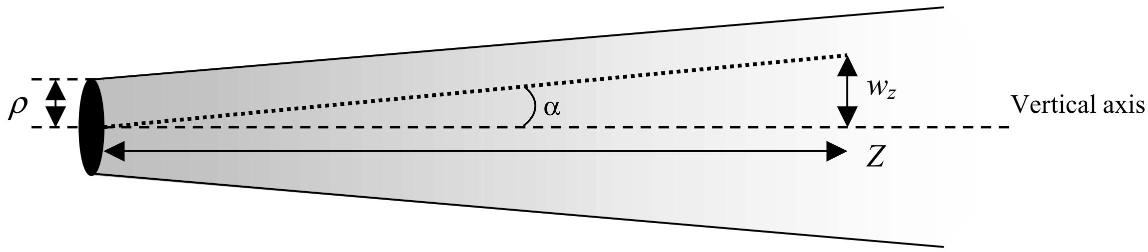

Fig. 9 *LED intensity profile*: Power received at a point with an arbitrary angle α from the vertical axis obeys the Lambertian law [28]

5.1 Coverage model

We define the coverage area of an FSO node as the area in which another FSO node can be (i) *aligned* and (ii) *reached* for communication. Thus, the area, points of which are within the LOS of the FSO node as well as receive enough light intensity to trigger a PD, is called the *coverage area* of the FSO node under consideration.

For a 2-d circular FSO node, the total coverage is dependent on the effective coverage area achieved by a single transceiver C, and the total number of transceivers n. The effective coverage area of a single transceiver C can be formulated based on two different possibilities of placing of the transceivers, as shown in Fig. 12. In Case I, coverage areas of two neighboring transceivers do not overlap while such an overlap takes place in Case II due to denser placement of transceivers. In our modeling of the communication coverage for the 2-d circular FSO node, we need to differentiate between these two cases, because another FSO node located within the overlapping areas will be receiving light intensity from both neighbor transceivers of the data sending FSO node. This will be particularly problematic during the LOS search and establishment phases as there is a need for distinguishing the light beams received from each of the contributing neighbor transceivers. Even though it is possible to distinguish between the light beams received from the neighbor transceivers by using various techniques (e.g. different wavelengths), we conservatively assume that communication is not possible in these overlapping areas. So, the effective coverage area of a single transceiver C (and hence the complete FSO node) is dependent on the size of the overlap areas.

In the following subsections, we will outline components of calculating the effective coverage area of a single transceiver C, which will then be used to model the coverage area of a 2-d circular FSO node in Section 5.2.

Table 1 Mathematical notations

Symbol	Meaning
n	Number of transceivers on the FSO node
r	Radius of the FSO node (cm)
ρ	Radius of a transceiver (cm)
ς	Radius of the receiver (cm)
γ	The radius of the transmitter (cm)
τ	Arc length between the edges of two neighbor transceivers (cm)
θ	Divergence angle[a] of a transceiver (Rad)
φ	Angular difference between two neighbor transceivers (Rad)
L	Coverage area of a transceiver (cm^2)
C	Effective coverage area of a transceiver (cm^2)
I	Interference area of two neighbor transceivers (cm^2)
R	Height of the triangle in the coverage area of a transceiver (cm)
$R_{\max}$	Maximum range reachable by the FSO node (cm)
P	Transmitter source power (dBm)
S	Sensitivity of the photo-detector receiver (dBm) (assumed -43dBm)
V	Visibility (km)
q	Particle distribution constant
λ	Optical signal wavelength (nm)
x	Side angle of the upper isosceles triangle within the interference area (Rad)
k	Length of the base side of the upper isosceles triangle (cm)
y	Vertex angle seeing the intersecting arc of the interference area (Rad)

[a]Our divergence angle definition refers to the half angle from the axis of light propagation.

5.1.1 *Coverage area of a single transceiver, L*

Coverage area of a transceiver on two-dimensions looks like a cone (i.e. the vertical projection of a lobe) [28]. Power received at any point in this cone is dependent on the quality of the FSO transmitter(s) of the transceiver. Also, another key factor to determine the transceiver's coverage area is the sensitivity threshold of a PD, since the received light intensity must be higher than this sensitivity to achieve a communication link. The *received light intensity, PD's sensitivity, atmospheric attenuation*, and *geometric attenuation* all together determine the maximum range $R_{\max}$ of the FSO transceiver.

Intensity/Power Profile. Various characteristics of the FSO transmitter affect the received light intensity. Assuming that there is no atmospheric attenuation and geometric spread,

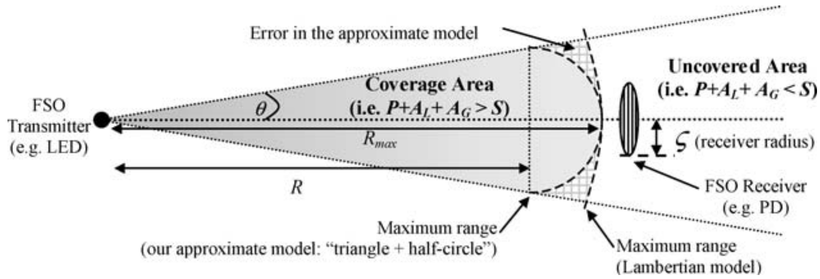

Fig. 10 *Maximum communication range of a single LED defines the border of the communication coverage area*: If the received power is greater than the receiver's sensitivity, then communication link can be established. If not, communication is not possible

the received light intensity at a point within the LOS of the transmitter is a function of the transmitter's source power P dBm, the radius of the transmitter γ cm, and the divergence angle of the transmitter θ Rad [28].

Smaller divergence angle of the transmitter shows the higher quality (strength) of the received light from it. Lasers operate with 0.5 m Rad to 2.5 m Rad divergence angles, while VCSELs with 2.5 m Rad to 75 m Rad and LEDs with 60 m Rad to 200 m Rad. As LEDs are the most inexpensive transmitters, we will use their intensity profile (which is worse than the lower divergence ones) in our analysis.

As shown in Fig. 9, LEDs intensity profile follows the Lambertian law [28], i.e. intensity is directly proportional to the cosine of the angle from which it is viewed. At a distance Z, let the received power on along the beam be P_Z. Based on the Lambertian law, at an arbitrary angle α from the vertical axis and at a distance Z, the intensity would be: $P_{\alpha,Z} = P_Z \cos(\alpha)$. For edge-emitting LEDs, this is improved by a factor u in the power of cosine, i.e. the intensity is given by: $P_{\alpha,Z} = P_Z \cos^u(\alpha)$.

Also, as a generic definition for all FSO transmitters, the beam radius w_Z at the vertical distance Z is defined as the radial distance at which the received power is $\frac{1}{e^2} P_Z$. So, the divergence angle θ is the special value of α, where the ratio $P_{\alpha,Z}/P_Z = 1/e^2$ holds, which means θ can be calculated by $\theta = \tan^{-1}(w_Z/z)$.

Calculation of the Maximum Range. Given an intensity profile as described above, we then determine the coverage area of a single transceiver as the area in the LOS of the transmitter where the received power is greater than the sensitivity threshold of the PD being used as the receiver. This threshold-based method defines the maximum reachable range for the transceiver. Note that the longest possible reachable range will be on the vertical axis of the transmitter as shown in Fig. 10. In addition to the Lambertian loss in the received power due to radial distance from the axis of propagation (see Fig. 9), atmospheric attenuation and geometric spread also causes loss in the received power, which we will include in our modeling in the next few paragraphs.

FSO propagation is affected by both the atmospheric attenuation A_L and the geometric spread A_G, which practically necessitates the source power to be greater than the power lost [28]. Each of these losses in power is described in detail below:

The *geometric attenuation* A_G is a function of transmitter radius γ, the radius of the receiver (on the other receiving FSO node) ς cm, divergence angle of the transmitter θ and the distance between the transmitting node and receiving node R [28]:

$$A_G = 10 \log \left(\frac{\varsigma}{\gamma + 200R\theta} \right)^2$$

The *atmospheric attenuation* A_L consists of absorption and scattering of the laser light photons by the different aerosols and gaseous molecules in the atmosphere. The power loss due to atmospheric propagation is given by Bragg's Law [28] as:

$$A_L = 10 \log(e^{-\sigma R})$$

where σ is the attenuation coefficient consisting of atmospheric absorption and scattering. For the wavelengths used for FSO communication, Mie scattering dominates the other losses, and therefore σ is given by [35]:

$$\sigma = \frac{3.91}{V} \left(\frac{\lambda}{550} \right)^{-q}.$$

In the above formulation of σ, V is the atmospheric visibility in kilometers, q is the size distribution of the scattering particles whose value is dependent on the visibility:

$$q = \begin{cases} 1.6, & V \geq 50\,\text{km} \\ 1.3, & 6\,\text{km} \leq V < 50\,\text{km} \\ 0.585\, V^{1/3}, & V < 6\,\text{km} \end{cases}$$

So, the maximum range $R_{\max}$ that can be reached by an FSO transceiver (or the maximum reachable range) is dependent on the transmitter's source power P dBm, the receiver's sensitivity S dBm, the radius of the transmitter γ cm, the radius of the receiver (on the other receiving FSO node) ς cm, the divergence angle of transmitter[2] θ mRad, the visibility V km, and the optical signal wavelength λ nm. [28].

For a conventional photo-detector (PD) sensitivity of $S = -43$ dBm [28, 31], the following inequality must be satisfied for the PD to detect the optical signal:

$$S - P < A_L + A_G - (P + 43) < A_L + A_G \quad (1)$$

Substituting for A_L [28] and A_G [28] leads us to the following inequality, maximum solution of which is $R_{\max}$:

$$-(P + 43) < 10\,\log(e^{-\sigma R}) + 10\,\log\left(\frac{\varsigma}{\gamma + 200R\theta}\right)^2. \quad (2)$$

Solving (2) for R yields the range where communication is possible between two FSO transceivers which includes an LED(s) transmitter with radius γ cm and a PD with radius ς cm. Thus, (1) and (2) define the relationship between various FSO propagation factors (such as visibility, divergence angle, receiver radius, transmitter radius) and the maximum reachable range $R_{\max}$. The transmitter and receiver radiuses γ and ς can be adjusted for the particulars of the transceiver being used on the design. As it will be detailed in Section 5.2.1 later, we will set those radiuses so that they match to the specifics of the transceiver design we use in the 2-d circular FSO nodes.

Approximation of the Coverage Area of a Single Transceiver. To make the computations easier for the rest of the paper, we approximated the coverage area of a transceiver with simple geometric shapes. This approximation helped us significantly in formulating the optimal coverage for the complete 2-d FSO node, which will be detailed in Section 5.2.

Specifically, we approximate an FSO transceiver's coverage area L as the combination of a triangle and a half circle, as shown in Figs. 10 and 12. As shown in Fig. 10, let R be the height of the triangle, which means the radius of the half circle is $R\tan\theta$. After finding $R_{\max}$ from (2), the height of the triangle within the coverage area of a transceiver R can be found by $R_{\max} = R + R\tan\theta$. Let L be the coverage area of a single transceiver, which can be derived as:

$$L = R^2\tan\theta + \frac{1}{2}\pi(R\tan\theta)^2 \quad (3)$$

Though the approximation eases computation complexity of the optimization problem in Section 5.2, it causes an error as shown in Fig. 10. We calculated the error caused by this approximation for the case when transmitter's source power P is 20 m Watts, PD sensitivity S is -43 dBm, transmitter radius is 0.3 cm, receiver radius is 0.5 cm, and visibility V is 20 km. Figure 11 shows the error (i.e. Lambertian model — the approximate model) for divergence angles up to 760 mRad.

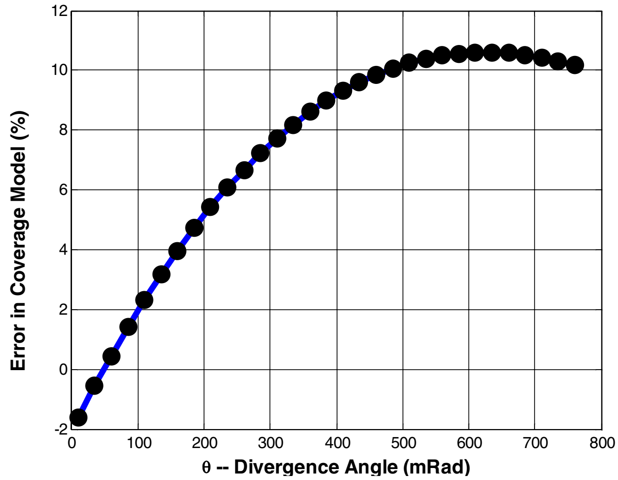

Fig. 11 *Error in the approximate model (i.e. Lambertian Coverage—Approximate Coverage)*: The approximate model yields no more than 11% for any FSO transmitter, and less than 7% error for most LEDs (i.e. $\theta < 250$ mRad). The model is underestimates the coverage area (i.e. conservative) for most FSO transmitters (i.e. $\theta > 50$ mRad), while it overestimates only for high-cost transmitters (i.e. $\theta < 50$ mRad)

As shown in Fig. 11, the error is less than 7% for a transmitter with 250 mRad divergence angle, which is a typical divergence angle for a regular LED. For very small divergence angles (i.e. < 50 mRad), the error becomes negative implying that the approximate model overestimates the coverage area. However for transmitters with divergence angles greater than 50 mRad the approximate model will be underestimating the coverage area, which means the model is conservative. We calculated the error for different transmitter source power P values and observed the same or very similar numbers. Overall, the model yields error less than 11% for all realistic divergence angle values and less than 7% for most of the LED transmitters, which means the error due to our "triangle + half-circle" approximation is negligible.

5.1.2 *Effective coverage area of a single transceiver, C*

Though each transceiver can have a coverage area L as defined in (3), the effective coverage area of a transceiver C on a 2-d circular FSO node will be less than L. Due to possible overlap of coverage areas of the neighbor transceivers, the effective coverage C may be less. In this subsection, we model this loss in the coverage to be conservative in our analysis.

[2] We assume the divergence angle the transmitter and field of view the receiver in a transceiver to be equivalent.

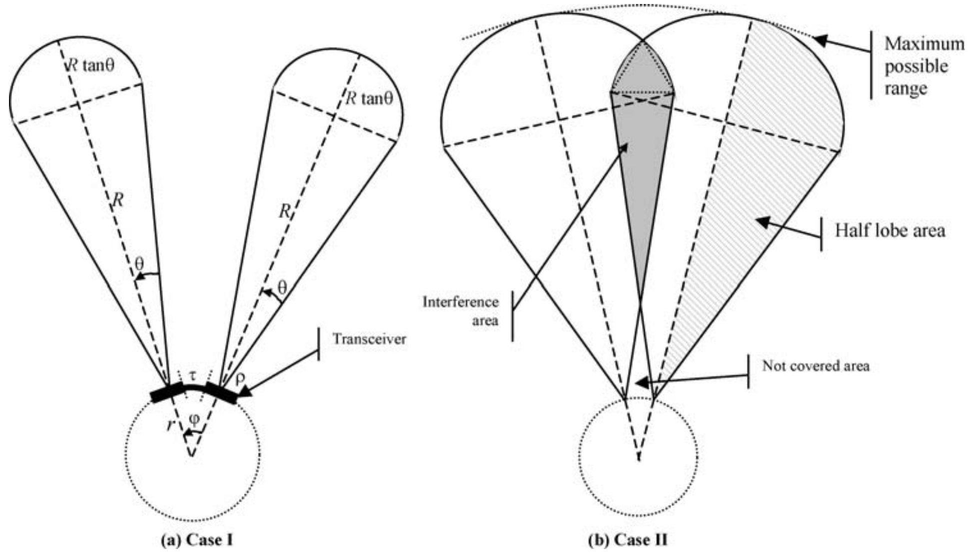

Fig. 12 *Coverage area of a 2-d circular FSO node.* (**a**) Coverage areas of neighboring transceivers do not overlap. (**b**) Coverage areas of neighboring transceivers overlap

Let r be the radius of the circular 2-d FSO node, ρ be the radius of a transceiver, and θ be the divergence angle of a transceiver. In each transceiver, we fix the radius of the transmitter to 2 mm and the remaining area is allocated to the receiver (see Fig. 14). A large receiver area can be obtained by suitable placing optics (e.g. a focusing lens of suitable aperture [36]) in front of the PD(s). We assume that the divergence angle of the transceiver θ is the minimum of the divergence angle of the transmitter and the field of view of the PD. Also, let τ be the length of the arc in between two neighboring transceivers on the 2-d circular FSO node. Assuming that n transceivers are placed at equal distance gaps on the circular FSO node, and since the diameter of a transceiver is 2ρ, the arc length along the circumference of the FSO node between the edges of two nearby transceivers can be calculated as follows:

$$\tau = \frac{2\pi r - n2\rho}{n} = 2\left(\frac{\pi r}{n} - \rho\right) \tag{4}$$

From (4), the angular difference φ between two neighboring transceivers can be derived:

$$\varphi = 360^\circ \frac{\tau}{2\pi r} \tag{5}$$

For the effective coverage area C of a single transceiver, two cases can happen based on the values of ϕ, θ, R, and r:

Case I. Coverage areas of the neighbor transceivers do not overlap, i.e. $R\tan\theta \leq (R + r)\tan(\varphi/2)$. In this case, the effective coverage area is equivalent to the coverage area, i.e. $C = L$.

Case II. Coverage areas of the neighbor transceivers overlap, i.e. $R\tan\theta > (R + r)\tan(\varphi/2)$. In this case, the effective coverage area is equivalent to the coverage area excluding the area that interferes with the neighbor transceiver. Let I be the interference area that overlaps with the neighbor transceiver's coverage, then $C = L - I$.

Notice that the interference area I is not fully useful for communication, since the signal the transceiver receiving is garbled by the presence of the signal from the adjacent transceiver(s) due to interference, unless we use WDM for the adjacent transceivers. LOS can still be achieved by selecting one of the transceivers for communication, however the other transceiver(s) receiving signal will be useless until the communication is over from the FSO node in the area I. Therefore, we do not count the area I in the coverage area, though this does not mean that those interference areas are totally ineffective.

Calculation of the interference area. As shown in Fig. 12(b), the interference area I is composed of two isosceles triangles and two leftover pies. To find the area I, the geometry for calculating the pieces of the area is needed. We need to find the angles x and y, and the length k, as shown in Fig. 13. From Fig. 13(a), we can write the following relationships:

$$x + \frac{\varphi}{2} = \frac{180 - y}{2} \tag{6}$$

$$\frac{k}{2\cos x} = 2R\tan\theta\sin\left(\frac{y}{2}\right) \tag{7}$$

From (5), (6), and (7), we find x and y, which means area of the upper isosceles triangle can be found. However, to do so, we still need to know the length k, which can be found by angles and lengths of the several triangles in Fig. 13(b):

$$k = 2\frac{R}{\cos\theta}\sin\left(\theta - \frac{\varphi}{2}\right) - 2r\sin\left(\frac{\varphi}{2}\right) \tag{8}$$

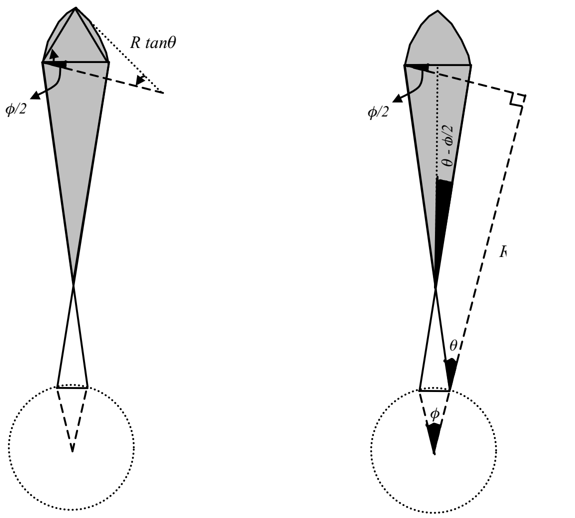

(a) Need to find the angles x and y. **(b)** Need to find the length k.

Fig. 13 A few key angles and lengths need to be found to find the interference area

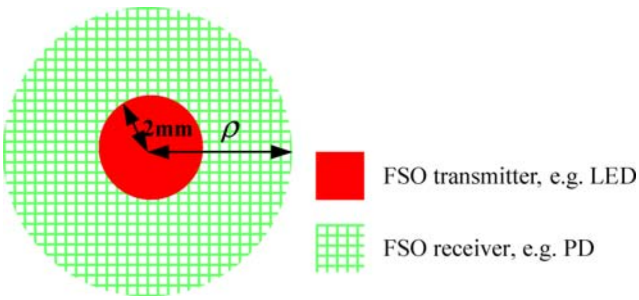

Fig. 14 *Transceiver design to be used in 2-d circular FSO nodes*: We assume that there is an LED-size transmitter at the center with a radius of 2 mm. The rest of the transceiver area is devoted to FSO receiver(s)

5.2 Optimal coverage

For given transmitter source power P, divergence angle θ, and visibility V, optimal number of transceivers that should be placed on the 2-d circular FSO node can differ. In particular, optimal number of transceivers (i.e. n) can be different based on the parameters P, θ and V as well as the metric to be optimized. We optimize the total effective coverage area nC of the 2-d circular FSO node, though other metrics (such as ratio of uncovered area and total possible area) can also be chosen. In addition to P, θ and V; the size of the FSO node (i.e. the radius of the FSO node circle r and the radius of a transceiver ρ) also plays a major role in the optimal number of transceivers n. Since C is dependent on P, θ, V and n; for given r and ρ, the optimization problem can be written as:

$$\max_{\theta, P, V, n} \{nC(\theta, P, V, n)\} \tag{9}$$

such that $0.5\,\text{mRad} \le \theta \le 250\,\text{mRad}$, $4\,\text{mWatt} \le P \le 32\,\text{mWatt}$, and $200\,\text{m} \le V \le 20,000\,\text{m}$.

Table 2 Parameters for optimization

Parameter	Meaning	Value(s) Min	Max
θ	Divergence angle of a transceiver (mRad)	0.5	250
P	Transmitter source power (mWatt)	4	32
V	Visibility (m)	200	20, 000
r	Radius of the FSO node (cm)	1	25
ρ	Radius of a transceiver (cm)	0.3	$r/2$

In our search for the best n, for a particular FSO node and transceiver size, we varied P, θ and V based on current FSO technology and literature, as shown in Table 2. Conventional lasers generate source power of 4–10 mW, and VCSELs and LEDs generate 4–30 mW. So, we varied P from 4 mW up to 32 mW. Similarly, we varied θ from 0.5 mRad up to 250 mRad, as lasers, VCSELs, and LEDs have divergence angles 0.5–2.5 mRad, 2.5–75 mRad, and 60–250 mRad respectively. Also, we varied the radius of the circular FSO node from 1 cm to 25 cm, which includes very small FSO node sizes (1–5 cm of radius) for indoor usage as well as large sizes (10–25 cm of radius) for outdoor usage. Finally, given a circular FSO node radius r cm, we varied the transceiver radius from 0.3 cm to $r/2$.

5.2.1 Transceiver design

Depending on the size of the 2-d circular FSO node, size of a possible transceiver can be larger than conventional FSO transmitter and receiver sizes. For example, for the largest circular FSO node we consider (i.e. $r = 25$ cm), the transceiver radius can be as large as 12.5 cm (i.e. $\rho = r/2$). Such transceiver radiuses are larger than conventional FSO transmitter or receiver sizes. However, it is possible to reach large transmitter/receiver sizes by using a mesh of them or by means of additional optical hardware or both. Examples of such FSO transceivers exist, e.g. [31, 32].

Since focus of our paper is not to design efficient transceivers, we will use a simple transceiver design for the rest of our analysis. Also, the specifics of the transceiver design does not significant effects on the main insights about the efficiency of dense packaging and optimality of the 2-d circular FSO nodes we are investigating in our analysis. The specific transceiver design we are using in the rest of our modeling is that it includes an FSO transmitter (e.g. LED) at the center and the rest of the transceiver's area is allocated to the FSO receiver (e.g. PD). Figure 14 shows the specific transceiver design we used in our calculations. We kept the FSO transmitter's radius constant at 2 mm while leaving the rest of the transceiver's area to receivers, i.e. PD(s).

5.3 Optimal coverage results

By applying the approach described in the previous section, we obtained optimal number of transceivers on a 2-d circular FSO node that maximizes the coverage area. To examine both small FSO node sizes (i.e. for indoors) and large sizes (i.e. for outdoors), we varied the FSO node radius r and the radius of a transmitter on the node ρ. Here, we report a subset of our results for the FSO node radius values of 1 cm, 2 cm, and 5 cm for *indoors*, and 15 cm and 20 cm for *outdoors*. Similarly, to examine different weather conditions, we varied the visibility V. We report a subset of our results for visibility of 0.2 km for *adverse*, 6 km for *normal*, and 20 km for *clear* weather.

Figure 15 shows the optimal number of transceivers n for three FSO node designs (one for indoors, and two for outdoors) for all weather conditions. Notice that the optimal n values reported in Fig. 15 are valid for all the three weather conditions (i.e. adverse, normal, and clear) we investigated. So, an interesting observation is that *the light source power P and the visibility V have little or no effect on the optimality of n*; rather, the geometric shape of the FSO node and the divergence angle plays the major role. This is a very important result since it means that optimum number of transceivers is pretty much *fixed* for a particular FSO node and transceiver size regardless of the visibility and the source power situation. This property of circular or spherical (the property can be shown to be valid for 3-d spheres) *FSO nodes allows adaptive tuning of the source power based on the actual visibility*.

Furthermore, as can be seen from Fig. 15, the relative size of the FSO node radius r and the transceiver radius ρ determines the shape of the optimal n as θ changes. Also, as expected, the optimal n reduces as θ decreases, though with steps at specific θ values corresponding to significant changes in the ratio of the interference area with respect to the total coverage area.

Another important metric for the FSO nodes is the maximum range $R_{\max}$ in which two such nodes can communicate. $R_{\max}$ depends on all parameters affecting the design. Particularly, lower θ or higher P leads to higher $R_{\max}$, and larger r or ρ leads to higher $R_{\max}$, as shown in Fig. 16.

5.4 Design recommendations

Value of the maximum communication range, $R_{\max}$, as well as the effective coverage, nC, for various FSO node designs is very important as it shows scalability of our circular 2-d FSO node designs for long distances and large coverage. To shed some light on the effects of FSO node's radius and transceivers' radius on the efficiency of the design in terms of $R_{\max}$ and nC, we investigated a few possible circular FSO node designs. Tables 3 and 4 show $R_{\max}$ and nC for 13 different designs with transceiver divergence angle 200 mRad and 75 mRad respectively. In terms of transmitters, 200 mRad

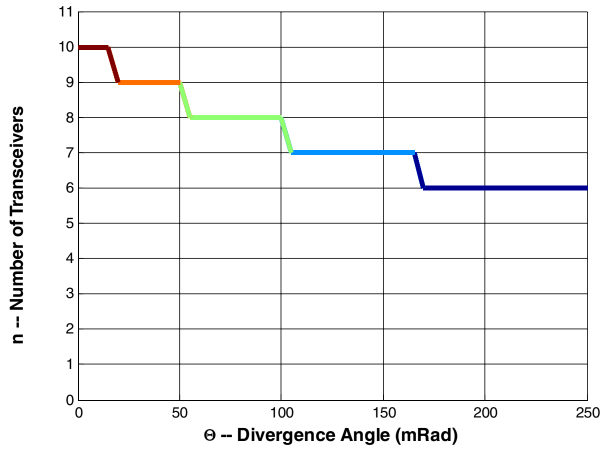

(a) $r = 1$cm, $\rho = 0.3$cm

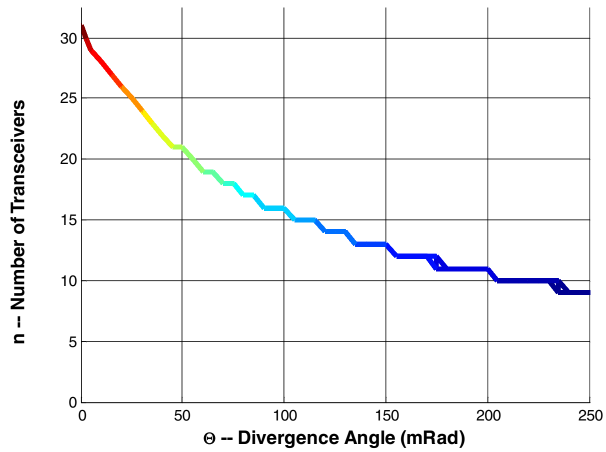

(b) $r = 25$cm, $\rho = 2.5$cm

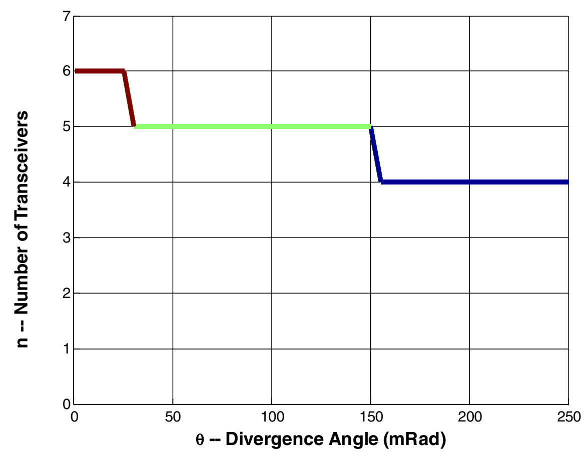

(c) $r = 25$cm, $\rho = 12.5$cm

Fig. 15 *Optimal n for three different FSO nodes at all weather conditions*: *The graphs are two-dimensional views of three-dimensional graphs* where an addition axis of the light source power P exists. The graphs are valid for all the three visibility conditions, i.e. $V = 0.2$ km, $V = 6$ km, and $V = 20$ km. Except little differences for a few values of the divergence angles in (c) above, the optimal number of transceivers is the same along the hidden axis P. The graphs show that the light source power P and visibility V have little or no effect on the optimality of n. The geometric shape of the FSO node (i.e. r and ρ) and the divergence angle determine the optimality of the total coverage

Fig. 16 *Maximum communication range depends on all parameters affecting the FSO node design*: Lower divergence angle or higher source power leads to higher communication range. Larger FSO node radius or transceiver radius leads to higher communication range

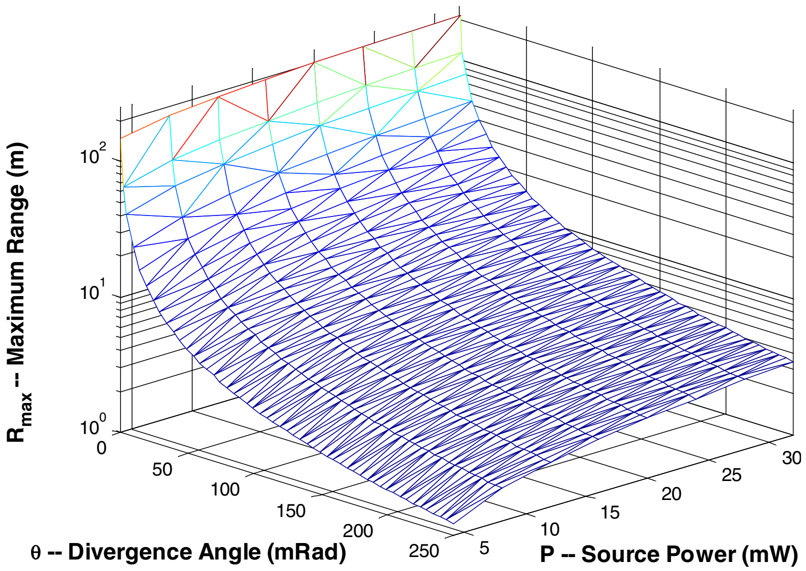

(a) $r = 1$cm, $\rho = 0.3$cm, $V = 0.2$km

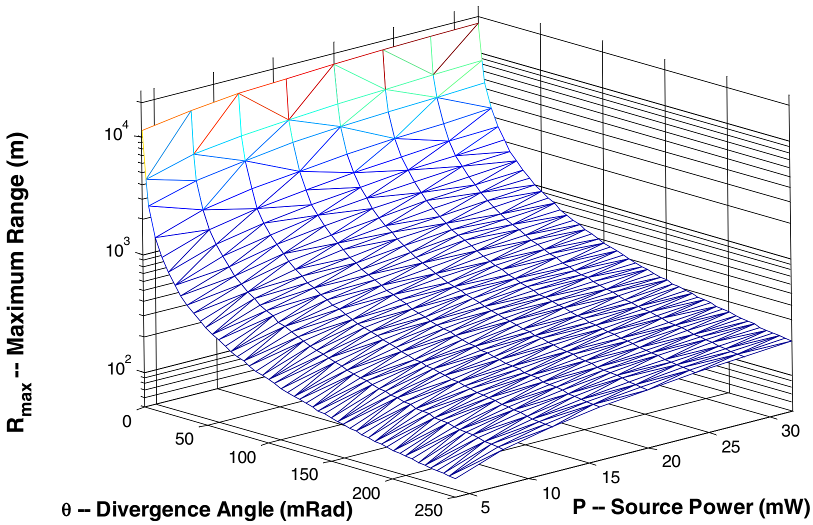

(b) $r = 25$cm, $\rho = 12.5$cm, $V = 20$km

corresponds to an average LED whilst 75 mRad corresponds to a low-quality VCSEL. To be conservative on the quality of the transceivers we picked such high divergence angles, even though it is possible to use very inexpensive FSO transmitters and receivers with very low divergence values, e.g. $\sim$20–30 mRad. As it can be seen from Tables 3 and 4, *the maximum communication range of the node depends solely on the area of the transceiver* (i.e. the radius ρ) for fixed θ and P.

Among the 13 designs, we recommend some of these designs for indoor usage (i.e. designs #1, #2, #3, #4, #6, #8, and #11) and other for outdoor usage (i.e. designs #7, #9, #10, #12, and #13). Though each design can serve a particular purpose based on the application, we marked the ones that we think fit best to indoor and outdoor usages. For example, designs #8 and #11 would be very good for using as a central hub attached to the ceiling of a crowded room as it can have lots of transceivers on it (i.e. with $\rho = 1.5$ cm and $\rho = 2.5$ cm respectively) while communication range can be maintained at the order of 40–50 m. Designs #4 and #6 would perform very well as a small device being attached to laptops or other mobile indoor devices where size of the system is not desired to be large. Design #2 can be used for very short distance mobile wireless indoor communication, e.g. connectivity among desktop computers in a large office with many tables. Similarly, assuming VCSEL quality transmitters (i.e. $\theta < 75$ mRad), design #13 can be used at mobile nodes needing long-range (>500 m) outdoor communication, such as ships and flying objects like helicopters. Designs #10 and #12 seems to provide

Table 3 Maximum communication range R_{max} and effective coverage nC for optimal FSO node designs with $\theta = 200$ mRad and $P = 32$ mWatts

Designs		Adverse Weather ($V = 0.2$ km)		Normal Weather ($V = 6$ km)		Clear Weather ($V = 20$ km)		Possible usage
ID	Node/Component Sizes (cm)	R_{max} (m)	nC (m^2)	R_{max} (m)	nC (m^2)	R_{max} (m)	nC (m^2)	
1	$r = 1, \rho = 0.3$	4.3	20.3	4.5	22.0	4.5	22.1	*Indoor*
2	$r = 1, \rho = 0.5$	8.4	52.5	9.1	61.5	9.1	61.7	*Indoor*
3	$r = 2, \rho = 0.4$	6.5	59.6	6.9	67.3	6.9	67.5	*Indoor*
4	$r = 2, \rho = 1.0$	16.6	204.4	19.4	279.4	19.5	281.9	*Indoor*
5	$r = 5, \rho = 0.3$	4.3	40.6	4.5	44.0	4.5	44.1	*Indoor*
6	$r = 5, \rho = 1.5$	23.6	616.4	29.4	958.9	29.6	971.8	*Indoor*
7	$r = 5, \rho = 2.5$	35.3	919.0	49.0	1, 773.7	49.5	1, 813.6	*Outdoor*
8	$r = 15, \rho = 1.5$	23.6	1, 037.4	29.4	1, 609.3	29.6	1, 630.8	*Indoor*
9	$r = 15, \rho = 5.0$	57.1	3, 400.2	96.7	9, 725.6	98.8	10, 159.2	*Outdoor*
10	$r = 15, \rho = 7.5$	73.2	3, 961.7	143.0	15, 103.1	147.6	16, 106.0	*Outdoor*
11	$r = 25, \rho = 2.5$	35.3	2, 323.8	49.0	4, 465.3	49.5	4, 565.1	*Indoor*
12	$r = 25, \rho = 7.5$	73.2	5, 942.6	143.0	22, 654.6	147.6	24, 159.1	*Outdoor*
13	$r = 25, \rho = 12.5$	96.9	6, 934.4	231.5	39, 618.9	243.9	43, 926.9	*Outdoor*

Table 4 Maximum communication range R_{max} and effective coverage nC for optimal FSO node designs with $\theta = 75$ mRad and $P = 32$ mWatts

Designs		Adverse Weather ($V = 0.2$ km)		Normal Weather ($V = 6$ km)		Clear Weather ($V = 20$ km)		Possible usage
ID	Node/Component Sizes (cm)	R_{max} (m)	nC (m^2)	R_{max} (m)	nC (m^2)	R_{max} (m)	nC (m^2)	
1	$r = 1, \rho = 0.3$	10.7	66.7	11.9	81.7	11.9	82.1	*Indoor*
2	$r = 1, \rho = 0.5$	20.1	146.1	24.2	212.9	24.3	215.3	*Indoor*
3	$r = 2, \rho = 0.4$	15.8	199.6	18.3	268.6	18.4	270.9	*Indoor*
4	$r = 2, \rho = 1.0$	36.5	484.5	51.3	956.9	51.9	979.5	*Indoor*
5	$r = 5, \rho = 0.3$	10.7	191.9	11.9	234.8	11.9	236.1	*Indoor*
6	$r = 5, \rho = 1.5$	49.0	1, 397.6	77.2	3, 466.3	78.6	3, 589.6	*Indoor*
7	$r = 5, \rho = 2.5$	68.2	1, 688.6	127.3	5, 892.7	131.1	6, 240.7	*Outdoor*
8	$r = 15, \rho = 1.5$	49.0	3, 137.3	77.2	7, 767.0	78.6	8, 042.8	*Indoor*
9	$r = 15, \rho = 5.0$	100.1	5, 093.9	245.7	30, 701.4	259.5	34, 249.5	*Outdoor*
10	$r = 15, \rho = 7.5$	121.6	5, 375.6	355.7	45, 970.3	384.6	53, 762.8	*Outdoor*
11	$r = 25, \rho = 2.5$	68.2	6, 070.0	127.3	21, 127.0	131.1	22, 372.2	*Indoor*
12	$r = 25, \rho = 7.5$	121.6	8, 601.0	355.7	73, 552.5	384.6	86, 020.5	*Outdoor*
13	$r = 25, \rho = 12.5$	151.5	8, 336.8	555.5	112, 154.7	626.2	142, 519.7	*Outdoor*

best value for medium-range (~100 m) and large-coverage (>10,000 m^2) outdoor usage where another communicating node can be found within few hundred meters, as in for the cars or other mobile vehicles in a city. Design #9, however, is good for more static outdoor wireless networks (e.g. mesh networks) where large-coverage is not a must but range is of importance.

Table 3 also shows that our FSO node designs can scale up to 243.9 m as the communication range for outdoors. It is noticeable that this communication range can be achieved by an FSO node with radius 25 cm covered with transceivers with divergence angle of 200 mRad and an aggregate source power of 32 mWatts. Note that these divergence angle and source power values are within the current technology limits of very inexpensive (e.g. $1 per piece) LEDs, and LEDs with better (lower divergence and higher power) can easily be produced with very small additional costs. Also, the designs in Table 3 illustrate the possibility of attaining very large coverage areas such as 43,926.9 m^2. It is also worthwhile to note that even a circular FSO node with radius 2 cm can reach ~10 m communication range within the current technological limits.

Similarly, by using slightly higher quality FSO components (e.g. cheap VCSELs with divergence angles roughly about 75 mRad), Table 4 shows that it is possible to reach communication ranges as long as 626.2 m and coverage areas as large as 142,519.7 m^2 by an FSO node with radius 25 cm. Also, a very small design with radius 2 cm can reach up to 51.9 m communication distance and 979.5 m^2 coverage area.

The total coverage nC area achieved by an FSO node also depends on the number of transceivers as well as the visibil-

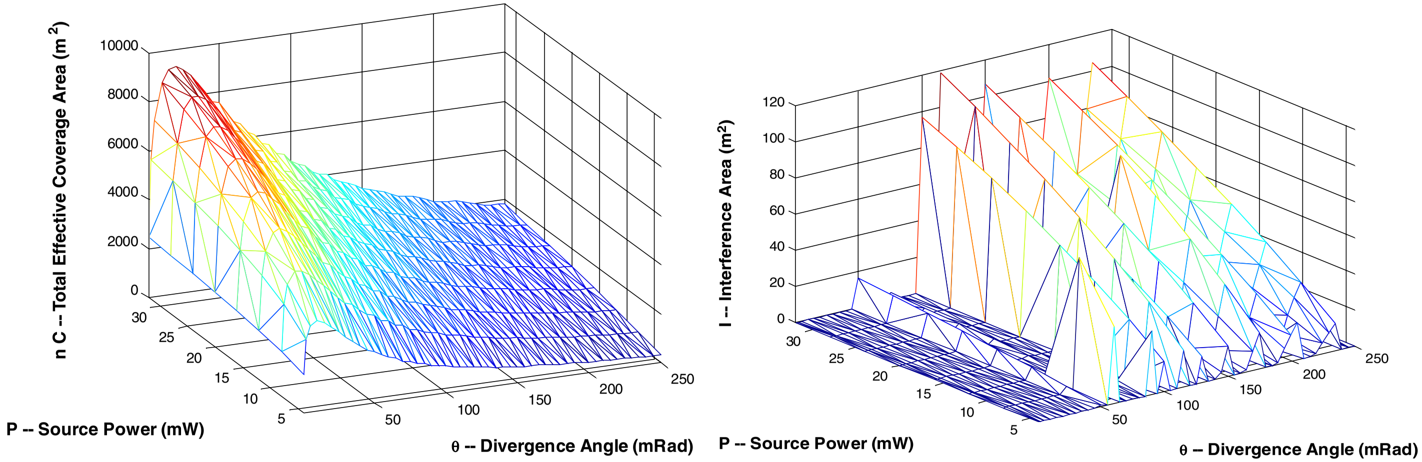

(a) Adverse weather, i.e. Visibility 0.2km

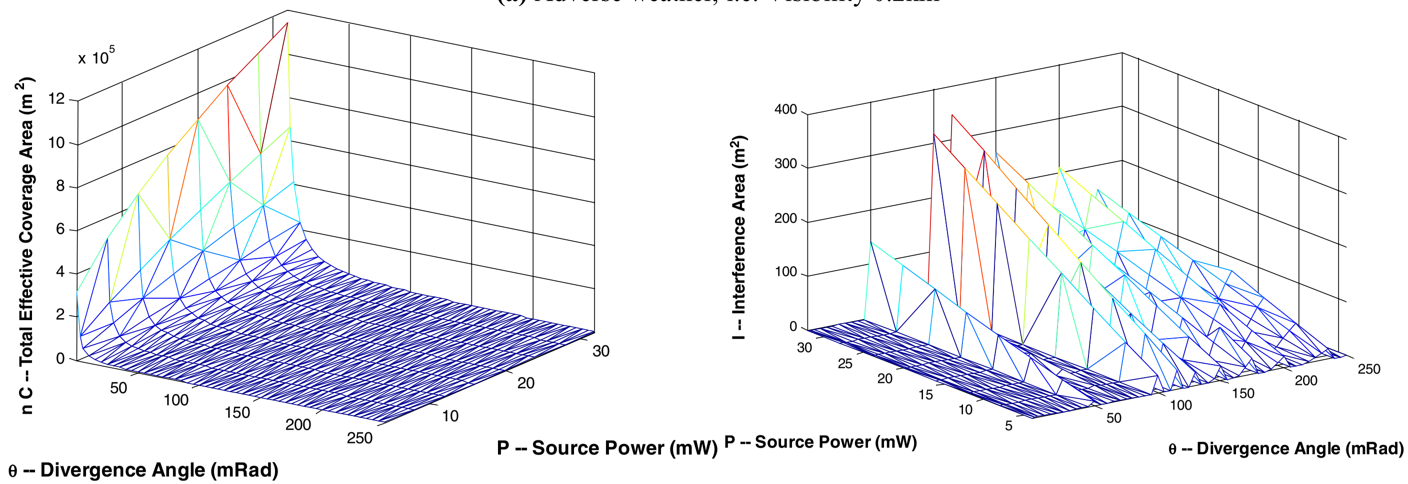

(b) Clear weather, i.e. Visibility 20km

Fig. 17 *Coverage area and interference area of an FSO node for* $r = 25$ cm *and* $\rho = 2.5$ cm: When the divergence angle is very small, the transceiver radius ρ limits the maximum number of transceivers and no interference between neighbors' transceivers exist. For higher divergence angles, maximum coverage can be obtained by having overlapping of coverage areas of neighbor transceivers as was shown in Fig. 12(b). Effect of changing the divergence angle is more severe on the coverage for more clear weather

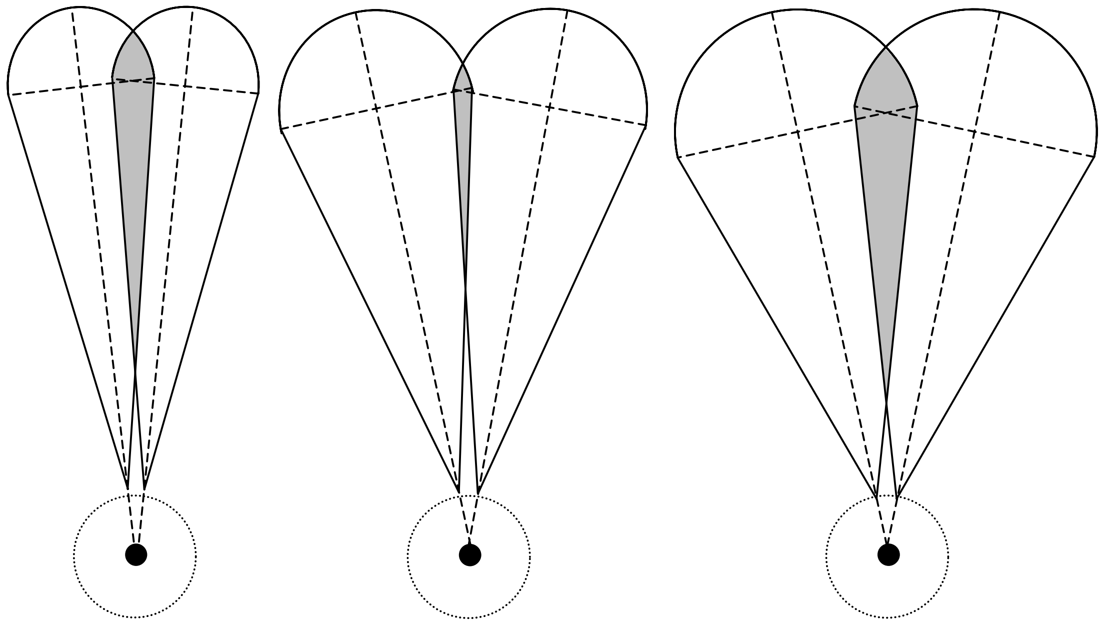

(a) Design I: θ_1, n_1 **(b) Design II:** θ_2, n_2 **(c) Design III:** θ_3, n_3

Fig. 18 *Optimal coverage and interference areas for different divergence angles are achieved by different number of transceivers*: Divergence angles of the transceivers increase from Design I to III, i.e. $\theta_1 < \theta_2 < \theta_3$. However, optimum number of transceivers to maximize coverage may not necessarily decrease (e.g. $n_1 > n_2 = n_3$), which causes the interference area to be oscillating as divergence angles vary

ity. As can be seen from the behavior of interference area in Fig. 17, the optimal number of transceivers is dependent on several factors which help minimize the fraction of interference area with respect to the total coverage area. When the divergence angle is very small, the transceiver radius ρ limits the maximum number of transceivers (since $2\pi r \leq n2\rho$ must be satisfied) and hence no overlap exists between the coverage areas of neighbor transceivers. For example, in Fig. 17, when the divergence angle is less than about 45 mRad (i.e. $\theta < 40$ mRad), the interference area I is equivalent to zero, showing that no overlap happens between the coverage of neighbor transceivers on the FSO node. For θ values allowing possible overlap between neighbor transceivers' coverage, our optimization results in optimal n values causing interference areas as shown in Fig. 17.

As can be observed by comparing Fig. 17(a) and (b), the total coverage behaves differently in different weather conditions as θ varies. Our results show that, by using transceivers with radius 1 cm and 32 mWatts *aggregate* light source power, an FSO node with radius 2 cm can cover a total of 484.5 m^2 in adverse weather and 979.5 m^2 in clear weather. *This result clearly shows scalability of our FSO node designs to very dense packaging of transceivers*. Similarly, by using transceivers with radius 12.5 cm and aggregate light source power 32 mRad, outdoor size FSO node designs with radius 25 cm can achieve a coverage area of 8,336.8 m^2 in adverse weather, 112,154.7 m^2 in normal weather, and 142,519.7 m^2 in clear weather.

As shown in Fig. 17, an interesting result is that *effect of increasing θ on the total coverage is more severe for higher visibility cases*. This is due to the fact that FSO propagation constructs a lobe-like shape which means majority of the coverage area is farther away from the light source. Again, as shown in Fig. 17, the interference area corresponding for the FSO node design optimized for maximum communication coverage oscillates as the divergence angle varies. More specifically, as the divergence angle increases the interference area may or may not increase. As explained in Fig. 18, the reason is that fraction of interference area to the actual coverage area determines the optimality of the number of transceivers in the design.

6 Summary

We proposed and developed a new scheme for mobile free space optical communications using (i) spherical surfaces tessellated with optical transceivers to obtain spatial reuse as well as angular diversity, and (ii) an auto-configurable optoelectronic circuit that makes use of this angular diversity to enable mobility between communicating nodes. The auto-configurable circuit monitors the LOS between two communicating spherical FSO nodes, and latches automatically onto existing LOS points. We built a proto-type system and demonstrated optical data transmission between mobile nodes. The basic techniques can be extended to configurations containing more than two nodes at longer distances. One key feature of our design is the absence of mechanical parts such as motors or moving mirrors typically used for auto-alignment purpose. This leads to significant savings in power consumption and improved reliability of our modules. We showed, through two-dimensional modeling, that this kind of free-space-optical system designs allow very dense packaging, and can scale to very long communication ranges as well as large coverage. Future work includes issues like optimal transceiver packaging patterns for desired coverage in three-dimensions, and application-specific designs of such systems.

Acknowledgment Authors would like to thank Mr. Chang Liu, Mr. Chingpo Chen, and Mr. David Partyka for thoughtful suggestions during various phases of this work. Authors would like to thank the anonymous reviewers for their invaluable comments which greatly helped in improving this paper. This work is funded by NSF grant number NSF-STI 0230787.

References

1. S. Acampora and S.V. Krishnamurthy, A broadband wireless access network based on mesh-connected free-space optical links, IEEE Personal Communications 6 (October 1999) 62–65.
2. J.W. Armstrong, C.Yeh and K.E. Wilson, Earth-to-deep-space optical communications system with adaptive tilt and scintillation correction by use of near-Earth relay mirrors, Optics Letters 23(14) (Optical Society of America, Washington, DC, July 1998), 1087–1089.
3. S. Arnon, Effects of atmospheric turbulence and building sway on optical wireless-communication systems, OSA Optics Letters 28(2) (January 2003) 129–131.
4. S. Arnon and N.S. Kopeika, Performance limitations of free-space optical communication satellite networks due to vibrations—analog case, SPIE Optical Engineering 36(1) (January 1997) 175–182.
5. S. Arnon, S.R. Rotman and N.S. Kopeika, Performance limitations of free-space optical communication satellite networks due to vibrations: direct detection digital mode, SPIE Optical Engineering 36(11) (November 1997) 3148–3157.
6. E. Bisaillon, D.F. Brosseau, T. Yamamoto, M. Mony, E. Bernier, D. Goodwill, D.V. Plant and A.G. Kirk, Free-space optical link with spatial redundancy for misalignment tolerance, IEEE Photonics Technology Letters 14 (February 2002) 242–244.
7. G.C. Boisset, B. Robertson and H.S. Hinton, Design and construction of an active alignment demonstrator for a free-space optical interconnect, IEEE Photonics Technology Letters 7 (June 1999) 676–678.
8. P. Djahani and J.M. Kahn, Analysis of infrared wireless links employing multibeam transmitters and imaging diversity receivers Communications, IEEE Transactions on Communications 48 (December 2000) 2077–2088.
9. G.E.F. Faulkner, D.C. O'Brien and D.J. Edwards, A cellular optical wireless system demonstrator, IEEE Colloquium on Optical Wireless Communications (1999) 12/1–12/6.
10. D.J. Goodwill, D. Kabal and P. Palacharla, Free space optical interconnect at 1.25 Gb/s/channel using adaptive alignment, Optical Fiber Communication Conference, 1999, and the International Conference on Integrated Optics and Optical Fiber Communication. OFC/IOOC '99. Technical Digest, Vol (2) (Feb 1999) pp 259–261.
11. D.J.T. Heatley, D.R. Wisely, I. Neild and P. Cochrane, Optical Wireless: The story so far, IEEE Communications 36 (December 1998) 72–74.
12. K. Ho and J.M. Kahn, Methods for crosstalk measurement and reduction in dense WDM systems, IEEE/OSA Journal of Lightwave Technology 14(6) (June 1996) 1127–1135.
13. J.M. Kahn and J.R. Barry, Wireless infrared communications, in: *Proceedings of the IEEE* (February 1997), Volume 85, pp. 265–298.
14. D. Kedar and S. Arnon, Backscattering-induced crosstalk in WDM optical wireless communication, IEEE/OSA Journal of Lightwave Technology 23(6) (June 2005) 2023–2030.
15. Lightpointe Inc., http://www.lightpointe.com/.
16. A.J.C. Moreira, R.T. Valadas and A.M.O. Duarte, Optical interference produced by artificial light, ACM/Kluwer Wireless Networks 3 (1997) 131–140.
17. M. Naruse, S. Yamamoto and M. Ishikawa, Real-time active alignment demonstration for free-space optical interconnections, IEEE Photonics Technology Letters 13 (Nov. 2001) 1257–1259.
18. D.C. O'Brien, et al. High-speed integrated transceivers for optical wireless, IEEE Communications Magazine 41 (March 2003) 58–62.
19. G. Pang, et al. Optical Wireless based on high brightness visible LEDs, IEEE Industry Applications Conference 3 (1999) 1693–1699.
20. A. Polishuk and S. Arnon, Communication performance analysis of microsatellites using an optical phased array antenna, SPIE Optical Engineering 42(7) (July 2003) 2015–2024.
21. R. Ramaswami and K. Sivarajan, *Optical Networks: A Practical Perspective* (Morgan Kaufmann Publishers, 2nd edition, 2001).
22. B.E.A. Saleh and M.C. Teich, *Fundamentals of Photonics* (Wiley-Interscience, 1 edition, 1991).
23. F. Shubert, Light-Emitting-Diodes-dot-org, http://www.rpi.edu/ ∼ schubert//Light-Emitting-Diodes-dot-org/.
24. A. Tavares, et al., Experimental characterization of rate-adaptive transmission and angle diversity reception techniques, IEEE Wireless Communications 10(2) (April 2003).
25. Terabeam Inc., http://www.terabeam.com/
26. H. Uno, K. Kumatani, H. Okuhata, I. Shrikawa and T. Chiba, ASK digital demodulation scheme for noise immune infrared data communication, ACM/Kluwer Wireless Networks 3 (1997) 121–129.
27. V. Vistas and A.C. Boucouvalas, Performance analysis of the advanced infrared (Air) CSMA/CA MAC Protocol for wireless LANs, ACM/Kluwer Wireless Networks 9 (2003) 495–507.
28. H. Willebrand and B.S. Ghuman, *Free Space Optics* (Sams Pubs, 1st edition, 2001).
29. Y.E. Yenice and B.G. Evans, Adaptive beam-size control scheme for ground-to-satellite optical communications, SPIE Optical Engineering 38(11) (November 1999) 1889–1895.
30. X. Zhu and J.M. Kahn, Free-space optical communication through atmospheric turbulence channels, IEEE Transactions on Communications (August 2002).
31. Terescope 10 Series, http://www.mrv.com/product/MRV-TS-004.
32. Cotco, Ultra Bright Red 5 mm LED, Model number LC503 AHR2 – 30P – A http://www.cotco.com/en/ led_lamps_list.asp? CATID = 2
33. *Cloudiness*, Gulf of Maine Ocean Observing System, http://www.gomoos.org/datatypes/CLOUDINESS.html
34. T.O. Drubay, R.K. Stevens, C.W. Lewis, D.H. Hern, W.J. Courtney, J.W. Tesch and M.A. Mason, Visibility and aerosol composition in Houston, Texas, Environ. Sci. Technol. 16(8) (1982) 514.
35. H.C. van de Hulst, *Light scattering by small particles* (Dover, New York, 1981).

36. fSONA: free Space Optical Network Architecture, http://www.fsona.com.
37. I.I. Kim, R. Stieger, J.A. Koontz, C. Moursund, M. Barclay, P. Adhikari, J. Schuster, E. Korevaar, R. Ruigrok and C. DeCusatis, Wireless optical transmission of fast ethernet, FDDI, ATM, and ESCON protocol data using the TerraLink laser communication system, Optical Engineering 37(12) (December 1998) 3143–3155.

Murat Yuksel is currently an Assistant Professor at the CSE Department of The University of Nevada - Reno (UNR), Reno, NV. He was with the ECSE Department of Rensselaer Polytechnic Institute (RPI), Troy, NY as a Postdoctoral Research Associate and a member of Adjunct Faculty until 2006. He received a B.S. degree from Computer Engineering Department of Ege University, Izmir, Turkey in 1996. He received M.S. and Ph.D. degrees from Computer Science Department of RPI in 1999 and 2002 respectively. His research interests are in the area of computer communication networks with a special focus on experimental networking, such as wireless ad-hoc networks, large-scale network simulation and experiment design, mobile ad-hoc free-space-optical (FSO) networks, network economics, and performance analysis. He is a member of IEEE and Sigma Xi.

Jayasri Akella obtained her Ph.D. from the Electrical, Computer, and Systems Engineering department at Rensselaer Polytechnic Institute, Troy, NY in 2006. She worked on multi-hop and mobile ad-hoc networks using free space optics for her Ph.D. thesis. She obtained her M.S. degree from the Indian Institute of Science, Bangalore, India, with a thesis on "Metrology using Optical Interference" in 1999. Her research interests include optical wireless communication, wireless ad-hoc networks, and photonics and its applications in engineering.

Shivkumar Kalyanaraman is a Professor at the Department of Electrical, Computer and Systems Engineering at Rensselaer Polytechnic Institute in Troy, NY. He holds a Computer Science B.Tech degree from IIT, Madras, India, and M.S., Ph.D. degrees from Ohio State University. His research interests include various traffic management topics and protocols for emerging tetherless networks. He is a member of the ACM and IEEE.

Partha Dutta is an Associate Professor at the Department of Electrical, Computer and Systems Engineering at Rensselaer Polytechnic Institute in Troy, NY. He holds a Computer Science B.S. degree in physics, chemistry, and mathematics from Bombay University, and M.S., Ph.D. degrees in physics from Indian Institute of Science. His research interests include semiconductors and nanotechnology. He has received two U.S. patents and has several more pending. He has published over 50 technical articles in high profile refereed journals and presented more than 40 talks in national and international conferences and meetings. His professional awards include the National Science Foundation Early Faculty CAREER Award in 2001, the Rensselaer Trustees Award for Faculty Achievement in 2001, the Martin Foster Award for Best Ph.D. Thesis of the Year in 1997, and the Young Scientist Award at the Eighth International Workshop on Physics of Semiconductor Devices, in Delhi, India, in 1995.